ACS OMEGA

Open Access

http://pubs.acs.org/journal/acsodf

Article

Optimized Chemical Bath Deposition for Low Cost, Scalable, and Environmentally Sustainable Synthesis of Star-Like ZnO Nanostructures

Gisella M. Di Mari, Valentina La Matta, Vincenzina Strano, Riccardo Reitano, Pierfrancesco Cerruti, Giovanni Filippone, Salvo Mirabella, and Elena Bruno*

Cite This: *ACS Omega* 2024, 9, 38591−38598

Read Online

ACCESS | Metrics & More | Article Recommendations

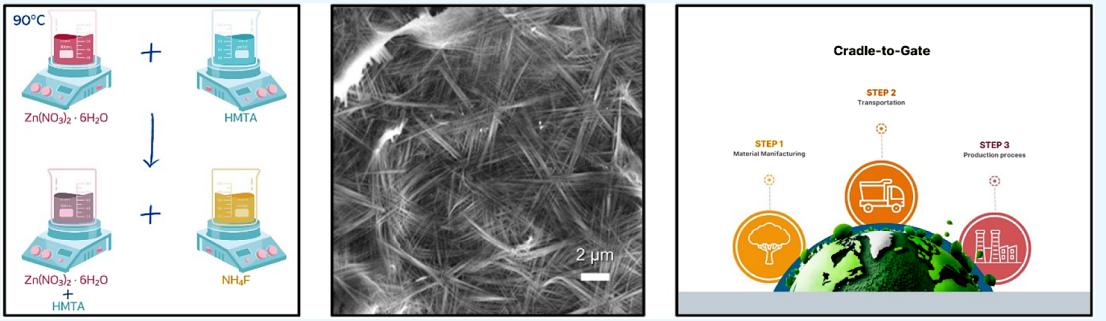

ABSTRACT: This paper highlights an affordable and straightforward method called chemical bath deposition (CBD) for generating different morphologies of ZnO-based nanostructures. In particular, a specific protocol was found to drive the growth versus a high-yield in-plane symmetric six-arm nanostructure, named a nanostar (NS). Each arm of the star consists of a cluster of parallel wires, creating a subnanostructure with a huge surface-to-volume ratio. As-grown NSs present a mixed phase of ZnOHF and ZnO, which converts to ZnO under thermal annealing at 300 °C. The NSs have a highly exposed surface area (13.2702 $m^2 \cdot g^{-1}$) and exhibit an energy gap of 3.25 eV. A cradle-to-gate life cycle assessment (LCA) analysis has shown the high ecofriendly potential of this synthesis route and identified hotspots that need to be addressed to minimize the environmental impact of NS synthesis on an industrial scale.

INTRODUCTION

Nanomaterials have been the subject of extensive research, driven not only by their fundamental scientific significance but also by their numerous technological applications.[1] Certainly, manipulating the dimensions and geometrical configurations of inorganic nanostructures holds significance both from a fundamental scientific perspective and for technological advancements, as it offers efficient approaches to modulate the electronic, magnetic, catalytic, and optical characteristics of materials.[2−4]

ZnO, a semiconductor material, finds diverse applications across field-effect transistor,[5] sensors,[6] energy systems,[7,8] biomedical applications,[9,10] and in biobased polymers and/or recycled plastics.[11−13] Indeed, ZnO stands out as a leading material due to its abundance, good transparency, high electron mobility, wide direct band gap of 3.37 eV, large exciton energy of 60 meV, and biocompatibility.[14] ZnO has also been demonstrated to be a biocompatible material: obtaining materials that are both abundant and biocompatible would substantially contribute to significant scientific advantages in various applications.[15−17]

The ability to produce ZnO nanostructures with a high yield (in order to easily obtain substantial quantities) is fundamental for applications where nanostructures are used to manipulate the phase morphology and, consequently, the properties of blends of bioplastics or recycled plastics. Numerous techniques are employed to obtain different ZnO morphologies, including electrochemical deposition,[18] metal organic chemical vapor deposition (MOCVD),[19] physical vapor deposition (PVD),[20] thermal evaporation,[21] chemical bath deposition (CBD),[22] and others. Among these methodologies, chemical bath deposition stands out as the most favorable choice due to its ability to

Received: April 29, 2024
Revised: June 12, 2024
Accepted: July 10, 2024
Published: September 4, 2024

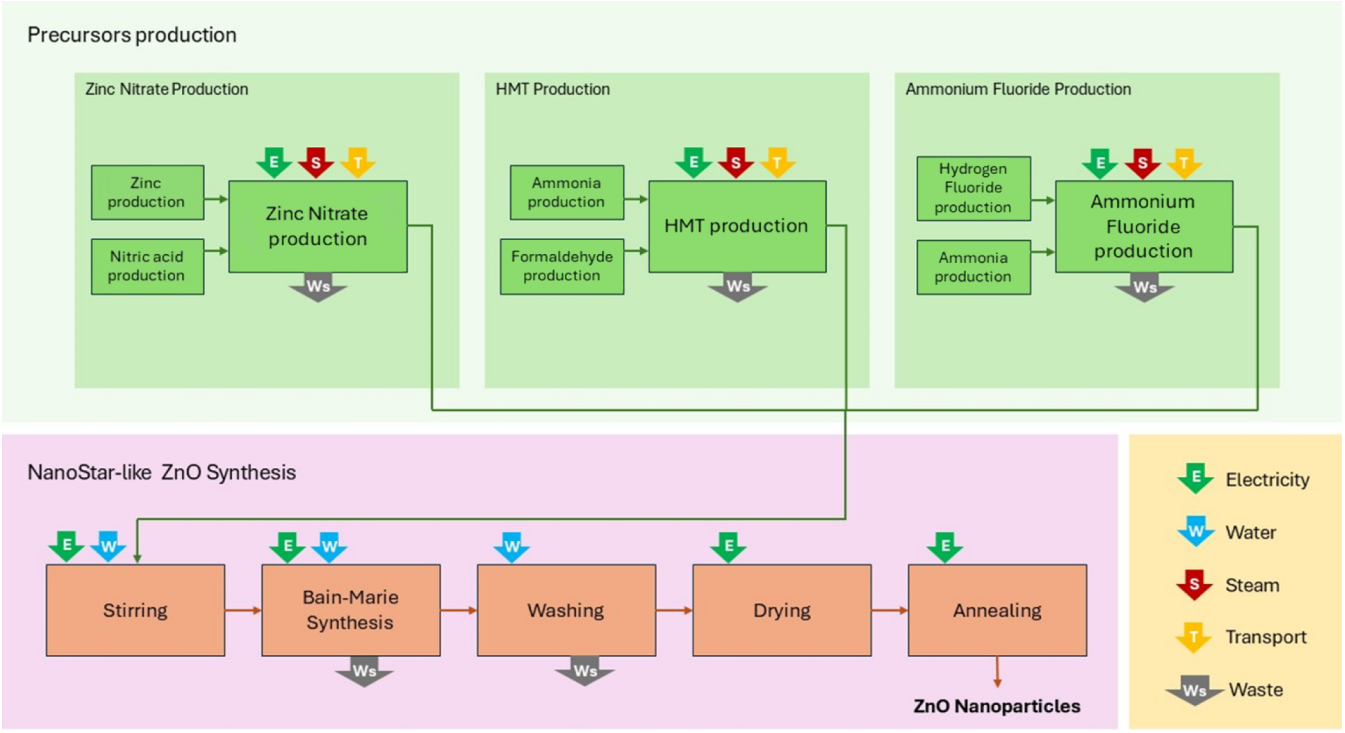

Figure 1. Scheme of modeling of the CBD synthesis process used for life cycle impact assessment.

easily modulate the morphology, structural characteristics, and optical properties of ZnO nanostructures.[23] Indeed, this method allows for the manipulation of various parameters, including precursor concentration, growth duration, and temperature.[24] On the other contrary, CBD offers the additional benefits of operating in mild conditions, enabling precise control over chemical composition, simplicity, and scalability for large-scale manufacturing.[25] Usually, synthesis in solution at higher pH values leads to higher production yields, as the process involves the formation of insoluble $Zn(OH)_2$, which precipitates, leading to a quasi-total conversion of zinc precursor into ZnO. However, at mild and slightly acidic pH levels, yields values are very poor, ranging from 20% to 30%.[26] Therefore, further studies are needed to improve these yields.

This paper reports a CBD approach for obtaining zinc oxide nanostructures in acidic pH environments using hexamethyleneteramine (HMTA), $Zn(NO_3)_2{\cdot}6H_2O$, and NH_4F water solutions, achieving competitive yields. Through meticulous study and control of process parameters, such as the order of reactant addition, it was possible to obtain zinc nanostructures with diverse morphologies (microflowers, nanoparticle-nanowire mixture, starlike structures, and belts). Among these nanostructures, particular attention was focused on a nanostar-shaped ZnO-based structure due to its innovative morphology, characterized by numerous crystalline wires organized within a shared plane in a highly ordered manner aligned at 60°, resulting in a very high exposed surface area (13.2702 $m^2{\cdot}g^{-1}$, evaluated through the Brunauer−Emmet−Teller method). As-grown nanostars were found to consist of a mixed structure of ZnOHF and ZnO, as evidenced by Raman analysis, and displayed an energy gap (E_g) of 3.25 eV. A cradle-to-gate life cycle assessment (LCA) investigation was hence performed on NS, using 1 $m^2{\cdot}g^{-1}$ NS BET surface area as the functional unit. The study aimed to identify the hotspots of the CBD process in preparation for possible scale-up from lab scale. The results highlighted the high ecofriendly potential of this synthesis route, demonstrating lower potential impact compared to lab-scale microwave-assisted methods. Further environmental benefits could be realized through optimization of the heating phase of the solution mixture, which is easily achievable on an industrial scale.

MATERIALS AND METHODS

Synthesis Procedure. All zinc oxide nanostructures were obtained by chemical bath deposition (CBD), employing water as the solvent. Three aqueous solutions, 25 mM HMTA, 25 mM $Zn(NO_3)_2{\cdot}6H_2O$, and 16 mM NH_4F, supplied by Merck-Sigma-Aldrich (Milan, Italy), were prepared by stirring them for 10 min each, and then separately heating them in a bain-marie configuration until reaching a final temperature of 90 °C. Then, the three precursors were combined in different orders while maintaining the bain-marie setup and the temperature. In one case, all reactants were mixed and stirred together for 10 min at room temperature. The entire solution was then placed in a bain-marie configuration until reaching a final temperature of 90 °C and maintained at 90 °C for 10 min. All the final solutions become opalescent within a few seconds and turn milky after approximately 5 min. After 10 min, the solutions were allowed to cool naturally, leading to the sedimentation of particulate matter at the bottom of the beaker. The solutions were then subjected to multiple deionized water washes by decantation. Subsequently, the powders obtained, with excess water removed, were placed in an oven at 100 °C for 24 h, in air, to dry. Selected powders were transferred to a quartz boat and subjected to annealing in an oven at 300 °C for 1 h under a nitrogen (N_2) flow, aimed at facilitating the transition from hydrated zinc forms obtained through the CBD synthesis to pure zinc oxide (ZnO) forms,[22,24] referred to with the prefix "Ann" in the following.

https://doi.org/10.1021/acsomega.4c04085
ACS Omega 2024, 9, 38591−38598

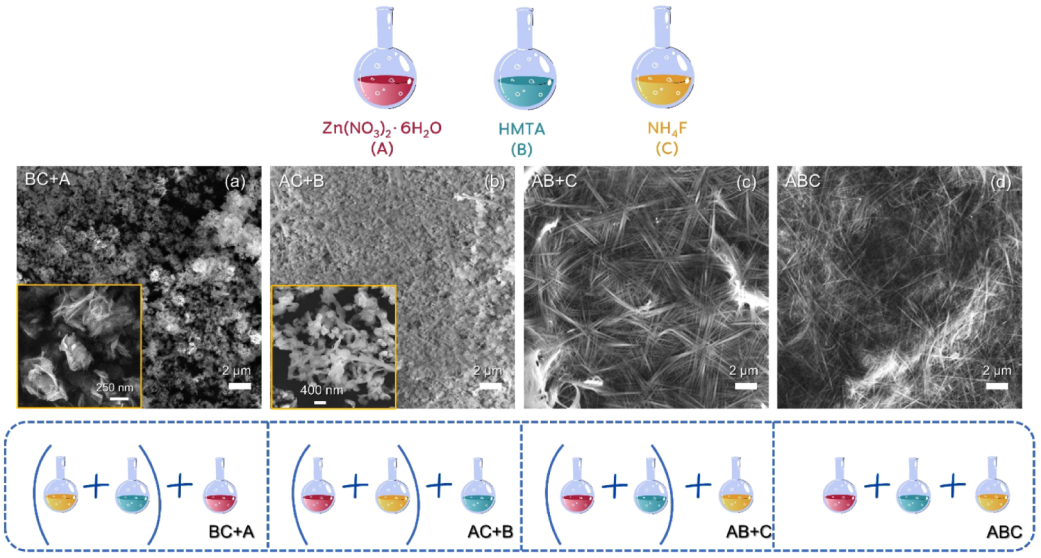

Figure 2. BC+A (a) microflower, AC+B (b) mixed nanoparticle-nanowire like, AB+C (c) nanostars, and ABC (d) belts like SEM images. Below is a schematic explaining how these different morphologies are obtained. The solution mixing for AB+C, AC+B, and BC+A occurs after all the reactant solutions reach 90 °C. For ABC the mixing occurs at room temperature, and then the solution is heated up to the temperature of 90 °C.

Characterization. The surface morphology of all nanostructures was assessed using scanning electron microscopy (SEM) (Gemini field emission SEM Carl Zeiss SUPRA 25, Carl Zeiss Microscopy GmbH, Jena, Germany).

SEM samples were prepared either by drop casting a few drops of the as-prepared synthesis solution sediment onto silicon substrates and subsequently drying them on a hot plate at 50 °C, or by directly applying some powders onto a carbon tape. Subsequently, the acquired SEM images were further analyzed using ImageJ software, which was employed to enhance both the brightness and contrast aspects.[27] Optical measurements were carried out using a LAMBDA 1050+ UV/vis/NIR spectrometer along with a 100 mm integrating sphere (PerkinElmer, Inc., Shelton, CT USA). Optical measurements were performed in a cuvette, using the specific nanostructure (NSs or AnnNSs) water suspension. Raman spectra were acquired using a LabRAM HR Horiba-Jobin Yvon spectrometer with a 632.8 nm laser source and an 1800 mm^{-1} grating, equipped with a confocal Olympus microscope. Raman samples were prepared by drop casting a few drops of NSs or AnnNSs solution onto Si substrates.

N_2 gas sorption measurements on NSs were carried out at 77 K using a Micromeritics 3Flex adsorption analyzer, in a relative pressure (p/p_0) range of 0.01−0.99. Prior to analysis, the sample (0.10 ± 0.01 g) was degassed at 80 °C under a vacuum for 10 h. The specific surface area (SSA) was determined by applying the Brunauer−Emmett−Teller (BET) equation[28] to the linear part of the absorption curve, using Micromeritics Flex 6.02 software.

Life Cycle Assessment Methodology. To assess the environmental impact of the CBD ZnO NanoStar-like synthesis, a cradle-to-gate life cycle assessment (LCA) study was conducted according to the principles and requirements of ISO 14040 and ISO 14044.[29,30]

The study was performed by considering 1 $m^2 \cdot g^{-1}$ of the BET surface area of the produced nanoparticles as the declared unit. The analysis includes (i) the preparation of the chemical precursors, (ii) their transportation to the facilities, and (iii) all the steps of laboratory synthesis, namely the stirring phase, bain-marie configuration synthesis, solution washing, drying and annealing in the oven. As shown in Figure 1, electricity, steam, and water consumption, emissions, and waste treatment were considered for each step. The study was carried out using OpenLCA software, and the Ecoinvent 3.1 database was used to model the background processes with reference to European average data. The parameters used for the life cycle inventory (LCI) were collected by measuring the energies involved during the synthesis process. As far as possible, electricity consumption was assessed by assuming full use of the equipment that required electricity. In particular, the use of the oven for the drying and annealing phase was normalized by assuming the maximum filling of the heating chamber. The same approach cannot be applied to the stirring and Bain-Marie synthesis phases, which were conducted with small-scale apparatuses that made it impossible to treat large amounts of chemicals at once. Regarding the production phases of the chemicals, ad hoc databases were modeled using the synthesis reactions reported in reference 31, starting from the base chemicals available in the Ecoinvent database and assuming stoichiometric balances. Moreover, as recommended in case of poor data availability,[32] the following typical chemical average production data were used for the modeling parameters: (i) yield of 95% for the chemical reaction; (ii) 2 MJ for thermal energy consumption in the form of steam; (iii) 0.333 kWh of electricity supply; (iv) a standard distance of 100 km by lorry and 600 km by train as transportation. Finally, the ReCiPe 2016 Hierarchist version of the impact assessment method was used to obtain comprehensive environmental data for the system under study.

RESULTS AND DISCUSSION

Reagents Combination Study. We thoroughly investigated how various synthesis parameters can affect the final nanostructure shape, focussing particularly on the sequence in which reagents are mixed and its impact on nucleation and nanostructure growth. The synthesis procedure remained consistent, with systematic alterations made only to the order of reagent mixing. Assuming:

https://doi.org/10.1021/acsomega.4c04085
ACS Omega 2024, 9, 38591−38598

$Zn(NO_3)_2{\cdot}6H_2O$ = A

HMTA = B

NH_4F = C

Four syntheses were performed: AB+C, AC+B, BC+A, and ABC. In the first three syntheses (AB+C, AC+B, and BC+A), two reagents were initially mixed at 90 °C, followed by addition of the third reagent after 5 s. The solution was then maintained at 90 °C for 10 min. In the fourth synthesis (ABC), all three reagents were combined in a cold state in the same beaker, and the solution was stirred and then heated in a water bath to 90 °C, followed by maintenance at this temperature for 10 min to promote nanostructure growth. Figure 2 illustrates schematics of all of these combinations.

Figure 2a−d shows SEM images of the syntheses described earlier, illustrating the respective reactant mixing orders. In Figure 2a, the combination CB and A features a typical microflower structure. The combination AC+B (Figure 2b), however, contains both particulate and filamentous structures termed mixed nanoparticle-nanowire. The structure of combination AB+C (Figure 2c) appears star-like, formed by many belts assembled and oriented along six directions, at an angle of 60° between each belt. The nanostars can be circumscribed within an 11 μm diameter circle. Lastly, the combination ABC (Figure 2d) contains belts randomly scattered across the plane. Microflowers, shown in Figure 2a, can be inscribed within a circle with a radius of 350 nm. Cauliflower structures, shown in Figure 2b, is made of branched wires, each hundreds of micrometers long, and nanoparticles with an average radius of 100 nm. Nanostar structures, depicted in Figure 2c, consist of 6 arms, each measuring 5 μm. Finally, Figure 2d displays random wires that are tens of micrometers long.

To elucidate the diverse nanostructures obtained, one must take into account the contributions of each of the three reagents to the growth of the nanostructure. Examining the initial step, when zinc nitrate is added to hexamethylenetetramine, the latter coordinates with Zn^{2+} ions, thereby controlling the concentration of free zinc ions in the solution. This combination is well known to promote the formation of zinc oxide nanorods, thanks to the equilibrium established in the solution, which promotes anisotropic growth along the (001) direction.[33] With the addition of ammonium fluoride to the reaction mixture, the fluoride anion acts as a counterion to the zinc coordination complex under acidic pH, immediately capturing the zinc present in solution. This addition, occurring just after the first two precursors, leads to the formation of a star-like structure, as depicted in Figure 2c. The nanostructure transition from flowers to ordered wires on the plane occurs. In the BC+A case, $Zn(NO_3)_2{\cdot}6H_2O$ is added afterward, causing the zinc ion to promptly bond with the fluoride anion, resulting in the classic nanosheet structure that collectively forms the nanoflower.[24] In the AB+C case, the scenario is different: $Zn(NO_3)_2{\cdot}6H_2O$ and HMTA are already dissolved in the solution. Zinc ions are immediately coordinated by the neutral ligand, HMTA. However, upon the addition of fluoride, it binds to the zinc cation, attracted by its positive charge. The steric hindrance imposed by the neutral HMTA ligands hampers the growth of the nanosheets. Nevertheless, this process leads to the formation of a distinct structure from the typical rods obtained through the reaction of equimolar amounts of $Zn(NO_3)_2{\cdot}6H_2O$ and HMTA. The structure generated, in fact, consists of multiple strips, orderly arranged on the plane forming a nanostar. NSs appear to exhibit a well-defined order on the plane, as the belts are not arranged randomly but intersect at 60° angles. As verified via SEM analysis, the morphology of the nanostructures remained unchanged after annealing at 300 °C in a N_2 atmosphere (not shown).

Role of Ammonium Fluoride on Nanostars Growth. Among the various nanostructures seen earlier, nanostars synthesized in the BC+A process exhibit an innovative and articulated shape. The visibly larger surface area compared to the other morphologies shown in Figure 2c could have high impact in the fields of sensing, energy production, and storage by electrochemical routes.[34,35]

In order to define how ammonium fluoride affects NS synthesis, we repeated the BC+A synthesis by varying the ammonium fluoride concentration (8, 16, and 32 mM NH_4F), keeping the concentrations of the other reactants unchanged. Figure 3a−f shows the nanostar SEM images at 8, 16, and 32 mM concentrations at low and high magnifications. All the three samples were prepared in the same way: by sampling from the bottom of the respective synthesis beaker and drop-casting the same number of drops onto Si substrates. The nanostar structure is not clearly defined for the lowest concentration in Figure 3a,d, whereas it is well-defined for concentrations equal to or higher than 16 mM. In the case of the highest concentration in Figure 3c, the nanostars seem to be halved in dimension compared to those at the medium 16 mM concentration in Figure 3b, with the average arm length decreasing from 5 μm (Figure 3b,e) to 2.5 μm (Figure 3c,f). Conversely, the nanostar density appears to increase from Figures 3a −c.

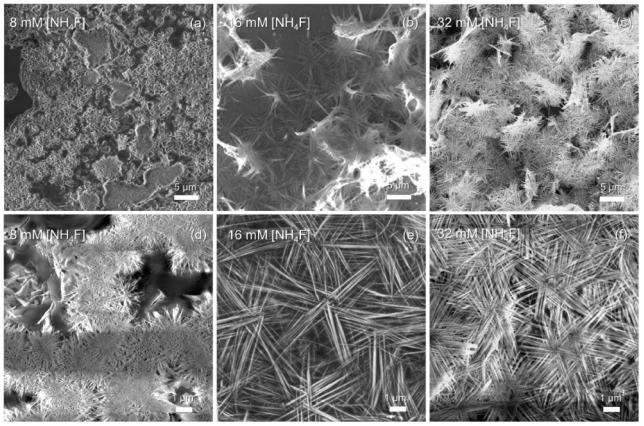

Figure 3. SEM images of nanostars using (a, d) half, (b, e) normal, and (c, f) double NH_4F concentration at low and high magnifications, respectively.

It appears evident that ammonium fluoride does not accelerate the growth kinetics but rather significantly influences NS nucleation and, consequently, the quantity of nanostars finally obtained. Conversely, with zinc nitrate remaining constant, there are more NSs at [NH_4F] 32 mM in terms of quantity, but they are smaller in dimension compared to those at 16 mM.

Nanostar Composition and Crystal Structure. Figure 4 represents the Raman spectra of NSs and AnnNSs. As proven from the Raman spectra, the as-grown NS is a heterostructure composed of ZnO[36] and ZnOHF.[37] Strong features appear at

https://doi.org/10.1021/acsomega.4c04085
ACS Omega 2024, 9, 38591−38598

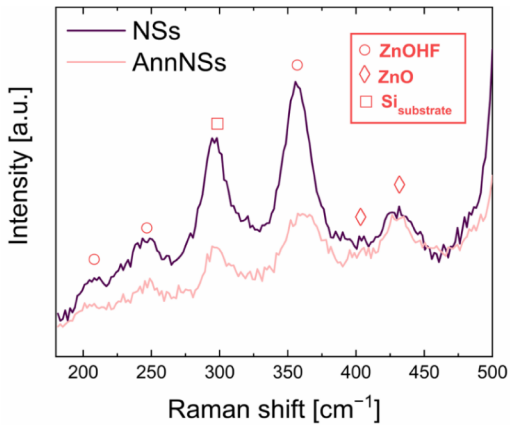

Figure 4. NSs and AnnNSs Raman spectra. Circle symbols identify the ZnOHF phase peaks,[36] while rumble symbols highlights the ZnO phase peaks.[37] Square symbols represent the Si substrate.[38]

approximately 158, 250, and 366 cm^{-1}, with the most intense peak originating from the ZnOHF structure, while the peaks at 410 and 436 cm^{-1} arise from the ZnO crystal structure. The 300 °C annealing procedure significantly degrades the ZnOHF phase, as can be evinced from the decreased intensity of its peaks, although some residual ZnOHF remains after thermal treatment.

Figure 5 shows the Tauc Plot, calculated by considering a direct and allowed transition for both NSs and AnnNSs,

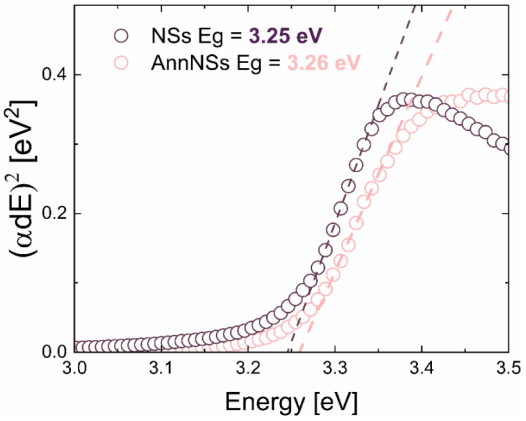

Figure 5. NSs and AnnNSs Tauc plots and the E_g values obtained.

extrapolated from the transmittance spectra of the nanopowder suspension in water, in the 200−800 nm wavelength range. The estimation of the energy band gap (E_g) was performed using the Tauc plot, defined as the x-intercept of the fitted line in the linear region of the Tauc plot.[39] An E_g of 3.25 eV was found for NSs, while AnnNSs possessed an E_g of 3.26. The lower E_g for both NSs and AnnNSs can be justified by considering a surface rich in defects, such as oxygen vacancies.[34] These vacancies create many levels close to the conduction band, which work as trapping levels for the electrons, thereby slightly lowering the optical band gap. Also, AnnNS possesses a slightly lower E_g than the ones reported in literature for bulk ZnO.[40] This can be justified with the presence of impurities of ZnOHF, as reported in the Raman spectra, and confirmed by XRD analysis.[34]

Figure 6 shows the nitrogen adsorption and desorption isotherms of the NSs. Moderate absorption at low relative

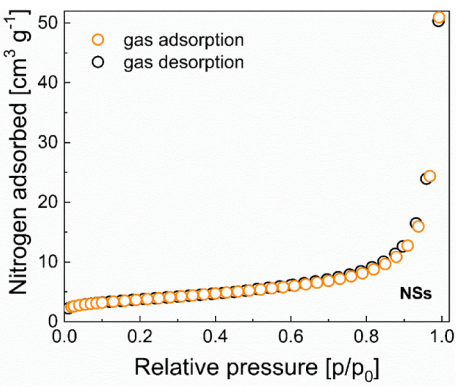

Figure 6. N_2 sorption isotherm of ZnO NSs.

pressure values was noted, along with the absence of sorption hysteresis. This behavior, classified as Type III shape according to IUPAC[41] is typical of macroporous absorbents with weak absorbate−adsorbent interactions, indicating that the NSs did not exhibit significant micro- or meso-porosity. Therefore, the specific surface area (SSA) value of 13.27 ± 0,03 $m^2 \cdot g^{-1}$, determined from such isotherms according to the Brunauer−Emmet−Teller (BET) equation, was ascribed to the very highly exposed surface of the ZnO NSs.

Yield Considerations. Further estimations regarding the powder yield still necessitate investigation, which could pave the way for large-scale applications of these nanostructures, such as in polymer blends. The assessment of ZnO synthesis yield was conducted for all four syntheses investigated. The estimation was done by assuming that the entire procedure was constrained by the availability of a Zn reactant, and by considering a 1:1 molar correlation between zinc nitrate and zinc oxide. Indeed, the annealing procedure at 300 °C under N2 flux for 1 h was conducted with the purpose of converting almost all ZnOHF into ZnO, as reported in other papers.[24,34] The powder yield was determined by quantifying the mass of nanostructures produced during a 10-min growth period following the 300 °C annealing process (supposing that only pure ZnO was present), relative to the initial amount of zinc nitrate used:

$$Zn(NO3)_2 \cdot 6H_2O \rightarrow ZnO + NO_x + H_2O$$

The yield results for the four syntheses are reported in Table 1. Nanostar yield could reach values up to 45% (see Table 1),

Table 1. Reagents Combination and Yield Estimation for all Samples

synthesis	combination	yield %
AB+C	A + B, then C	35
AC+B	A + C, then B	30
BC+A	B + C, then A	45
ABC	A + B + C (room T)	39

as suggested by the molar ratio between ZnO and zinc nitrate, demonstrating the superiority of NSs over the other three morphologies realized also from this point of view. The 45% yield value we obtained in a solution with a pH of 5.7 is very interesting and promising for future large-scale production efforts, considering that similar or higher yields have been obtained only under strongly alkaline conditions, whereas in

https://doi.org/10.1021/acsomega.4c04085
ACS Omega 2024, 9, 38591−38598

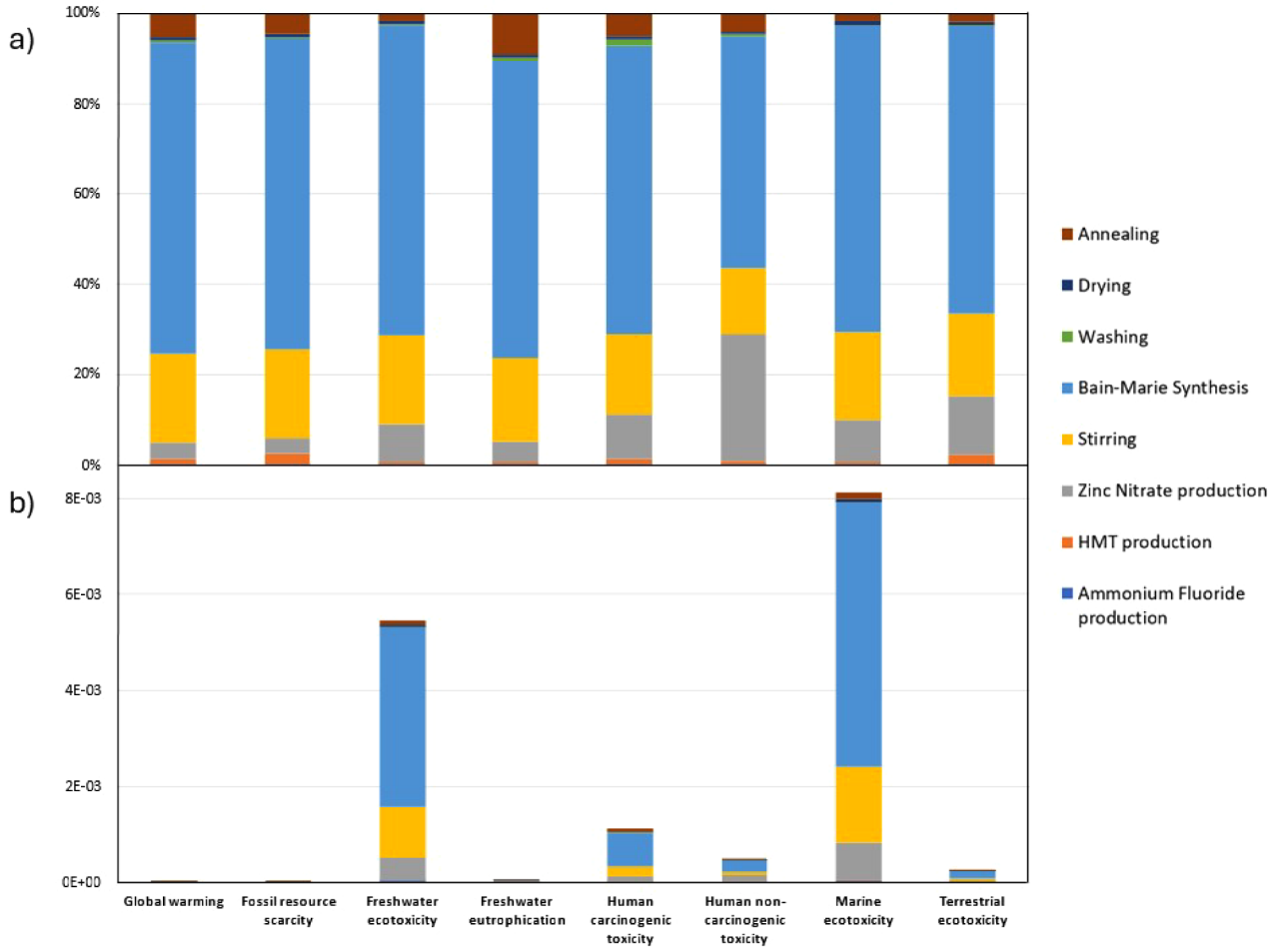

Figure 7. Graphical representation of eight selected ReCiPe 2016 (H) Midpoint Categories for the eight process steps included in the boundaries and listed in the legend on the right side. (a) Relative contribution of the single phase to the total category amount (b) Hierarchist version with World (2010) H normalization for the same impact categories.

acid conditions the yields reported in literature are around 30%.[26]

Life Cycle Impact Assessment. The environmental impacts of CBD synthesis have been detailed at the ReCiPe Midpoint level using eight indicators, namely global warming, fossil resource scarcity, freshwater ecotoxicity and eutrophication, human carciogenic and noncarciogenic toxicity, marine and terrestrial ecotoxicity. This type of study is very important for identifying any critical steps in the synthesis process that are necessary for real sustainable large-scale applications. Regarding the relative contributions of the single steps of the process in Figure 7a, heating the solution mixture in a bain-marie configuration dominates all impact categories. Other relevant contributions come from the stirring phase and zinc nitrate production. This key compound has the highest impact among the chemicals used. Figure 7b shows the Hierarchist version with World (2010) H normalization for the selected impact categories. The comparison indicates that CBD synthesis is particularly critical in terms of marine and freshwater ecotoxicity, followed by human toxicity indicators. These results can be compared with those of Papadaki et al.,[42] who performed an LCA study on lab-scale synthesis of ZnO nanoparticles using a microwave-assisted technique with comparable BET surface area. The CBD synthesis adopted in the present study shows lower impacts than the above-mentioned microwave-based approach across all eight selected categories, with substantial reductions in marine ecotoxicity (−35%) and human toxicity (−60%) indicators. The overall impacts, however, remain much higher than those achievable at industrial scale, in which well-designed synthesis processes and production plants can ensure drastic reductions of emissions and energy demand.[43] The LCA analysis highlighted how water's high specific heat capacity renders heating via a hot plate highly energy-intensive. Nevertheless, at the industrial scale, nearly all generated heat is effectively channeled and recuperated, underscoring the efficiency of large-scale processes. Therefore, we can affirm that the NSs reported in this paper hold great promise for sustainable implementation on a large-scale in biobased polymers, recycled plastics, green energy applications, or biosensing.

CONCLUSIONS

In conclusion, this study presents an optimized, cost-effective chemical bath deposition method for producing zinc oxide-based nanostars (NSs) with a competitive yield of 45% under slightly acidic conditions. The distinct roles of the employed reagents HMTA, $Zn(NO_3)_2{\cdot}6H_2O$, and NH_4F in shaping and sizing the final nanostructure were examined. Specifically, introducing ammonium fluoride only after the coordination of Zn with the neutral ligand HTMA results in a structure

https://doi.org/10.1021/acsomega.4c04085
ACS Omega 2024, 9, 38591−38598

different from the typical rod formation observed in reactions involving equimolar amounts of $Zn(NO_3)_2{\cdot}6H_2O$ and HMTA. The resulting nanostars, characterized by a well-defined pattern on the plane consisting of bundles of belts oriented at 60° angles, display an exceptionally high surface-to-volume ratio, making them suitable for applications where this parameter is crucial, such as sensing or energy production and storage through electrochemical routes or biobased polymers and/or recycled plastics. NSs exhibit a unique morphology and optical properties, combined with a competitive yield. The LCA study highlighted challenges related to the energy-intensive bain-marie configuration, which can be easily overcome through industrial heat recovery approaches. This study paves the way for large-scale and environmentally sustainable applications of ZnO NSs in the fields of energy, sensing, and bioplastics.

AUTHOR INFORMATION

Corresponding Author

Elena Bruno − *Dipartimento di Fisica e Astronomia "Ettore Majorana", Università degli Studi di Catania, Catania 95123, Italy; CNR-IMM, Catania (University) Unit, Catania 95123, Italy*; Email: elena.bruno@dfa.unict.it

Authors

Gisella M. Di Mari − *Dipartimento di Fisica e Astronomia "Ettore Majorana", Università degli Studi di Catania, Catania 95123, Italy; CNR-IMM, Catania (University) Unit, Catania 95123, Italy;* orcid.org/0000-0002-1513-9684

Valentina La Matta − *Dipartimento di Ingegneria Chimica, dei Materiali e della Produzione Industriale (INSTM Consortium UdR Naples), University of Naples Federico II, Naples 80125, Italy*

Vincenzina Strano − *CNR-IMM, Catania (University) Unit, Catania 95123, Italy;* orcid.org/0000-0003-2053-4141

Riccardo Reitano − *Dipartimento di Fisica e Astronomia "Ettore Majorana", Università degli Studi di Catania, Catania 95123, Italy; CNR-IMM, Catania (University) Unit, Catania 95123, Italy*

Pierfrancesco Cerruti − *CNR-IPCB, Pozzuoli 80078, Italy*

Giovanni Filippone − *Dipartimento di Ingegneria Chimica, dei Materiali e della Produzione Industriale (INSTM Consortium UdR Naples), University of Naples Federico II, Naples 80125, Italy;* orcid.org/0000-0002-4382-3686

Salvo Mirabella − *Dipartimento di Fisica e Astronomia "Ettore Majorana", Università degli Studi di Catania, Catania 95123, Italy; CNR-IMM, Catania (University) Unit, Catania 95123, Italy;* orcid.org/0000-0002-9559-4862

Complete contact information is available at: https://pubs.acs.org/10.1021/acsomega.4c04085

Funding

This work was supported by programma ricerca di Ateneo UNICT 2020−22 linea 2 PIA.CE.RI "NaTI4Smart Sviluppo di NAnomateriali e Tecnologie Innovative per Smart detection", and by PRIN 2017 "CLEAN-Valorizing Sustainable Plastics through a CLEver use of NANoparticles" 20174FSRZS_003.

Notes

The authors declare no competing financial interest.

ACKNOWLEDGMENTS

The authors wish to thank G. Pantè, C. Percolla, and S. Tatì (CNR-IMM Catania, Italy) for the technical support.

REFERENCES

(1) Nasrollahzadeh, M.; Sajadi, S. M.; Sajjadi, M.; Issaabadi, Z. An Introduction to Nanotechnology. *Interface Sci. Technol.* **2019**, *28*, 1−27.

(2) Shouli, B.; Liangyuan, C.; Dianqing, L.; Wensheng, Y.; Pengcheng, Y.; Zhiyong, L.; Aifan, C.; Liu, C. C. Different Morphologies of ZnO Nanorods and Their Sensing Property. *Sens. Actuators, B* **2010**, *146* (1), 129−137.

(3) Anas, S.; Mangalaraja, R. V.; Ananthakumar, S. Studies on the Evolution of ZnO Morphologies in a Thermohydrolysis Technique and Evaluation of Their Functional Properties. *J. Hazard. Mater.* **2010**, *175* (1−3), 889−895.

(4) Ge, M. Y.; Wu, H. P.; Niu, L.; Liu, J. F.; Chen, S. Y.; Shen, P. Y.; Zeng, Y. W.; Wang, Y. W.; Zhang, G. Q.; Jiang, J. Z. Nanostructured ZnO: From Monodisperse Nanoparticles to Nanorods. *J. Cryst. Growth* **2007**, *305* (1), 162−166.

(5) Arnold, M. S.; Avouris, P.; Pan, Z. W.; Wang, Z. L. Field-Effect Transistors Based on Single Semiconducting Oxide Nanobelts. *J. Phys. Chem. B* **2003**, *107* (3), 659−663.

(6) Zhu, L.; Zeng, W. Room-Temperature Gas Sensing of ZnO-Based Gas Sensor: A Review. *Sens. Actuators, A* **2017**, *267*, 242−261.

(7) Theerthagiri, J.; Salla, S.; Senthil, R. A.; Nithyadharseni, P.; Madankumar, A.; Arunachalam, P.; Maiyalagan, T.; Kim, H.-S. A review on ZnO nanostructured materials: Energy, environmental and biological applications. *Nanotechnology* **2019**, *30*, 392001.

(8) Kumar, B.; Kim, S. W. Energy Harvesting Based on Semiconducting Piezoelectric ZnO Nanostructures. *Nano Energy* **2012**, *1* (3), 342−355.

(9) Jiang, J.; Pi, J.; Cai, J. The Advancing of Zinc Oxide Nanoparticles for Biomedical Applications. *Bioinorg. Chem. Appl.* **2018**, *2018*, 1062562.

(10) Singh, K. R.; Nayak, V.; Singh, J.; Singh, A. K.; Singh, R. P. Potentialities of Bioinspired Metal and Metal Oxide Nanoparticles in Biomedical Sciences. *RSC Adv.* **2021**, *11* (40), 24722−24746.

(11) Mallakpour, S.; Javadpour, M. The Potential Use of Recycled PET Bottle in Nanocomposites Manufacturing with Modified ZnO Nanoparticles Capped with Citric Acid: Preparation, Thermal, and Morphological Characterization. *RSC Adv.* **2016**, *6* (18), 15039−15047.

(12) Singh, A. K.; Bedi, R.; Kaith, B. S. Composite Materials Based on Recycled Polyethylene Terephthalate and Their Properties − A Comprehensive Review. *Composites, Part B* **2021**, *219* (April), 108928.

(13) Carroccio, S. C.; Scarfato, P.; Bruno, E.; Aprea, P.; Dintcheva, N. T.; Filippone, G. Impact of nanoparticles on the environmental sustainability of polymer nanocomposites based on bioplastics or recycled plastics − A review of life-cycle assessment studies. *J. Cleaner Prod.* **2022**, *335* (April 2021), 130322.

(14) Li, D.; Haneda, H. Morphologies of Zinc Oxide Particles and Their Effects on Photocatalysis. *Chemosphere* **2003**, *51* (2), 129−137.

(15) Li, Z.; Yang, R.; Yu, M.; Bai, F.; Li, C.; Wang, Z. L. Cellular Level Biocompatibility and Biosafety of ZnO Nanowires. *J. Phys. Chem. C* **2008**, *112* (51), 20114−20117.

(16) Dincă, V.; Mocanu, A.; Isopencu, G.; Busuioc, C.; Brajnicov, S.; Vlad, A.; Icriverzi, M.; Roseanu, A.; Dinescu, M.; Stroescu, M.; Stoica-Guzun, A.; Suchea, M. Biocompatible Pure ZnO Nanoparticles-3D Bacterial Cellulose Biointerfaces with Antibacterial Properties. *Arab. J. Chem.* **2020**, *13* (1), 3521−3533.

(17) Dagdeviren, C.; Hwang, S.-W.; Su, Y.; Kim, S.; Cheng, H.; Gur, O.; Haney, R.; Omenetto, F. G.; Huang, Y.; Rogers, J. A. Transient, Biocompatible Electronics and Energy Harvesters Based on ZnO. *Small* **2013**, *9* (20), 3398−3404.

(18) Li, G.-R.; Lu, X.-H.; Zhao, W.-X.; Su, C.-Y.; Tong, Y.-X. Controllable Electrochemical Synthesis of Ce4+-Doped ZnO

Nanostructures from Nanotubes to Nanorods and Nanocages. *Cryst. Growth Des.* **2008**, *8* (3), 1276−1281.
(19) Ye, J.; Gu, S.; Zhu, S.; Chen, T.; Hu, L.; Qin, F.; Zhang, R.; Shi, Y.; Zheng, Y. The Growth and Annealing of Single Crystalline ZnO Films by Low-Pressure MOCVD. *J. Cryst. Growth* **2002**, *243* (1), 151−156.
(20) Jimenez-Cadena, G.; Comini, E.; Ferroni, M.; Vomiero, A.; Sberveglieri, G. Synthesis of Different ZnO Nanostructures by Modified PVD Process and Potential Use for Dye-Sensitized Solar Cells. *Mater. Chem. Phys.* **2010**, *124* (1), 694−698.
(21) Zheng, J. H.; Jiang, Q.; Lian, J. S. Synthesis and Optical Properties of Flower-like ZnO Nanorods by Thermal Evaporation Method. *Appl. Surf. Sci.* **2011**, *257* (11), 5083−5087.
(22) Scuderi, M.; Strano, V.; Spinella, C.; Nicotra, G.; Mirabella, S. Low-Cost Synthesis of Pure ZnO Nanowalls Showing Three-Fold Symmetry. *Nanotechnology* **2018**, *29*, 135707.
(23) Tong, Y.; Liu, Y.; Dong, L.; Zhao, D.; Zhang, J.; Lu, Y.; Shen, D.; Fan, X. Growth of ZnO Nanostructures with Different Morphologies by Using Hydrothermal Technique. *J. Phys. Chem. B* **2006**, *110* (41), 20263−20267.
(24) Strano, V.; Greco, M. G.; Ciliberto, E.; Mirabella, S. Zno Microflowers Grown by Chemical Bath Deposition: A Low-Cost Approach for Massive Production of Functional Nanostructures. *Chemosensors* **2019**, *7* (4), 62.
(25) Baviskar, P. K.; Nikam, P. R.; Gargote, S. S.; Ennaoui, A.; Sankapal, B. R. Controlled Synthesis of ZnO Nanostructures with Assorted Morphologies via Simple Solution Chemistry. *J. Alloys Compd.* **2013**, *551*, 233−242.
(26) Komarneni, S.; Bruno, M.; Mariani, E. Synthesis of ZnO with and without Microwaves. *Mater. Res. Bull.* **2000**, *35* (11), 1843−1847.
(27) Schneider, C. A.; Rasband, W. S.; Eliceiri, K. W. NIH Image to ImageJ: 25 Years of Image Analysis. *Nat. Methods* **2012**, *9* (7), 671−675.
(28) Brunauer, S.; Emmett, P. H.; Teller, E. In Multimolecular. *J. Am. Chem. Soc.* **1938**, *60* (2), 309−319.
(29) ISO. *ISO 14040:2006* ISO 37456 @ Www.Iso.Org, 2006; pp 20. https://www.iso.org/standard/37456.html.
(30) ISO *38498 @ Www.Iso.Org* 2006; pp 46 https://www.iso.org/standard/38498.html.
(31) Quantity, P. Symbols and Units. *Nucl. Phys.* **1956**, *1* (8), 541−556.
(32) Hischier, R.; Hellweg, S.; Capello, C.; Primas, A. Establishing Life Cycle Inventories of Chemicals Based on Differing Data Availability. *Int. J. Life Cycle Assess.* **2005**, *10* (1), 59−67.
(33) Cosentino, S.; Fiaschi, G.; Strano, V.; Hu, K. J.; Liao, T. W.; Hemed, N. M.; Yadav, A.; Mirabella, S.; Grandjean, D.; Lievens, P.; Shacham-Diamand, Y. Role of AuxPt1-x Clusters in the Enhancement of the Electrochemical Activity of ZnO Nanorod Electrodes. *J. Phys. Chem. C* **2017**, *121* (29), 15644−15652.
(34) Di Mari, G. M.; Mineo, G.; Franzò, G.; Mirabella, S.; Bruno, E.; Strano, V. Low-Cost, High-Yield ZnO Nanostars Synthesis for Pseudocapacitor Applications. *Nanomaterials* **2022**, *12* (15), 2588.
(35) Di Mari, G. M.; Spadaro, M. C.; Salutari, F.; Arbiol, J.; Bruno, L.; Mineo, G.; Bruno, E.; Strano, V.; Mirabella, S. Low-Cost, High-Yield Zinc Oxide-Based Nanostars for Alkaline Overall Water Splitting. *ACS Omega* **2023**, *8* (40), 37023−37031.
(36) Khan, A. Raman Spectroscopic Study of the ZnO Nanostructures. *J. Pak. Mater. Soc.* **2010**, *4* (1), 5−9.
(37) Tian, H.; Li, Y.; Zhang, J.; Ma, Y.; Wang, Y.; Wang, Y.; Li, Y.; Cui, Q. High Pressure Induced Phase Transformation through Continuous Topology Evolution in Zinc Hydroxyfluoride Synthesized via a Hydrothermal Strategy. *J. Alloys Compd.* **2017**, *726*, 132−138.
(38) Lee, W. J.; Chang, Y. H. Growth without Postannealing of Monoclinic VO2 Thin Film by Atomic Layer Deposition Using VCl4 as Precursor. *Coatings* **2018**, *8* (12), 431.
(39) Raciti, R.; Bahariqushchi, R.; Summonte, C.; Aydinli, A.; Terrasi, A.; Mirabella, S. Optical Bandgap of Semiconductor Nanostructures: Methods for Experimental Data Analysis. *J. Appl. Phys.* **2017**, *121* (23), 234304.
(40) Özgür, Ü.; Alivov, Y. I.; Liu, C.; Teke, A.; Reshchikov, M. A.; Dǒan, S.; Avrutin, V.; Cho, S. J.; Morkoç, H. A Comprehensive Review of ZnO Materials and Devices. *J. Appl. Phys.* **2005**, *98* (4), 041301.
(41) Panzella, L.; Cerruti, P.; Ambrogi, V.; Agustin-Salazar, S.; D'Errico, G.; Carfagna, C.; Goya, L.; Ramos, S.; Martín, M. A.; Napolitano, A.; D'Ischia, M. A Superior All-Natural Antioxidant Biomaterial from Spent Coffee Grounds for Polymer Stabilization, Cell Protection, and Food Lipid Preservation. *ACS Sustainable Chem. Eng.* **2016**, *4* (3), 1169−1179.
(42) Papadaki, D.; Foteinis, S.; Mhlongo, G. H.; Nkosi, S. S.; Motaung, D. E.; Ray, S. S.; Tsoutsos, T.; Kiriakidis, G. Life Cycle Assessment of Facile Microwave-Assisted Zinc Oxide (ZnO) Nanostructures. *Sci. Total Environ.* **2017**, *586*, 566−575.
(43) Stieberova, B.; Zilka, M.; Ticha, M.; Freiberg, F.; Caramazana-González, P.; McKechnie, J.; Lester, E. Sustainability Assessment of Continuous-Flow Hydrothermal Synthesis of Nanomaterials in the Context of Other Production Technologies. *J. Cleaner Prod.* **2019**, *241*, 118325.

https://doi.org/10.1021/acsomega.4c04085
ACS Omega 2024, 9, 38591−38598